

Magnetization dynamics in arrays of strongly interacting magnetic nanocrystals

Tamar Telem-Shafir and Gil Markovich^{a)}

School of Chemistry, Raymond and Beverly Sackler Faculty of Exact Sciences, Tel Aviv University, Tel Aviv 69978, Israel

(Received 1 August 2005; accepted 27 September 2005; published online 23 November 2005)

Arrays of 6.6 nm iron oxide nanocrystals coated with fatty acid molecules were produced using the Langmuir-Blodgett technique. The arrays had a varying number of layers stacked together, going from two dimensional to three dimensional and two different in-plane interparticle separations. While temperature-dependent ac susceptibility measurements of the isolated nanocrystals obeyed the Néel-Brown relaxation law, the array relaxation deviated significantly from this simple law. This deviation together with the observed dc field influence on the susceptibility-temperature curves, the large shifts in blocking temperatures and reduction in susceptibility-temperature curve widths on going from isolated particles to the arrays indicated collective magnetization dynamics during magnetization freezing. A scaling law analysis of this freezing dynamics yielded different powers for the two different interparticle separations with no dependence on dimensionality. In spite of the spin-glass-like behavior, it is possible that small, magnetically ordered domains of nanocrystals form at low temperature. © 2005 American Institute of Physics. [DOI: 10.1063/1.2126663]

I. INTRODUCTION

Systems of interacting single-domain magnetic nanoparticles have been at the focus of many studies in the past decades.¹⁻³ These systems are interesting for their fundamental physical properties, which are linked to their application in magnetic data storage, magnetic-resonance imaging, and ferrofluids.

Until recent years, extensive work has been carried out on magnetic nanoparticles dispersed in solid matrices⁴ or on frozen ferrofluids³ where nanoparticle concentrations were varied as a mean to tune average interparticle separation and thus change the strength of interactions. These studies resulted in a variety of models and even contradictory conclusions, probably due to the large diversity of nanoparticle compositions, sizes, size distributions, and aggregation states between different samples.

More recently, with advances in colloidal chemistry⁵ and vapor deposition techniques⁶ magnetic nanoparticles could be arranged in arrays with a better-defined particle size and interparticle separation. Thus, with ordered magnetic nanocrystal arrays it should be possible to study in a rigorous way the influence of the dimensionality of the system and the strength of interactions between the magnetic nanocrystals on the measured magnetic properties.

The more interesting part of such studies is that of strongly interacting magnetic nanocrystals, where the interparticle dipolar interaction energy exceeds the individual particles' magnetic anisotropy energy. Then the interaction energy cannot be simply treated as a small correction to the effective potential barrier influencing the individual particle magnetization.⁷ In order to prepare such a system, the uniform magnetic nanocrystals must be brought to close prox-

imity. This can be done using organically capped colloidal magnetic nanocrystals,⁸ while with vapor deposition techniques it is far more difficult to obtain close packing while maintaining nanoparticle uniformity and only relatively large separations can be achieved.⁹

One of the key questions regarding the dynamics of magnetization switching in interacting magnetic nanoparticle systems is that of collective switching of ensembles of magnetic particles versus the static picture of individual nanoparticle response. In the limit of weak interactions and large single-particle magnetic anisotropy, the magnetization dynamics in the system can be described by switching of individual particles in a local field created by the neighbor particles that switch at different rates.⁷ However, it is clear that in the limit of strong dipolar interactions relative to the magnetic anisotropy barriers, in the case of a relatively uniform array, the dynamics cannot be described by such a static picture and collective magnetization dynamics must occur. The collective dynamics domain size (correlation length) is determined by the temperature, average value of dipolar energy, and uniformity in particle size and interparticle separation distances in the nanoparticle arrays. In addition, the characteristics of glassy magnetization dynamics, including phenomena such as aging and memory effects, have been observed in systems of interacting magnetic nanoparticles at low enough temperatures and discussed in the context of spin glasses.^{1,10-13}

Whether interparticle magnetic dipole-dipole interactions would lead to magnetic ordering or a spin-glass-like phase at low but finite temperature depends on the dimensionality and order in magnetic nanocrystal arrays. Magnetic disorder could be the result of a random distribution of anisotropy axes in cases of large magnetic anisotropy relative to the dipolar interaction energy. In the reverse case of strong

^{a)}Electronic mail: gilmar@post.tau.ac.il

dipolar interactions in hexagonal arrays magnetic disorder could be the result of frustration between magnetic moments due to particle size distribution and positional disorder.

In this work we present the results of magnetic measurements performed on relatively uniform iron oxide nanocrystal arrays with varying dimensionality, from two dimensional (2D) to three dimensional (3D) and varying interparticle separations, and compare those to measurements of noninteracting nanoparticles. The Langmuir-Blodgett (LB) technique was used to produce macroscopically uniform nanocrystal monolayers, which were crucial for this study. The magnetic measurement results show that in these arrays the interparticle interactions cannot be considered merely a perturbation to the anisotropy energy barriers. Rather, the nanocrystals are in the strong interactions regime, with the interaction energy being three to five times stronger than the single-particle anisotropy energy. In these arrays collective dynamics occur, accompanied by a spin-glass-like behavior at low temperatures.

Furthermore, the compatibility of the susceptibility data with the expressions used to describe spin-glass behavior, the Vogel-Fulcher law and a power law, was tested.

II. EXPERIMENTAL SECTION

A. Nanocrystals' preparation and characterization

The oleic-acid-capped iron oxide nanoparticles were synthesized according to Sun *et al.*¹⁴ Although originally described as magnetite nanocrystals by Sun *et al.*, their compositions probably had the general formula $\text{Fe}_{3-\delta}\text{O}_4$.^{15,16} Transmission electron microscope (TEM) images of the nanocrystals were analyzed and the average diameter of the nanocrystals estimated as 6.6 ± 2.0 nm. A dilute sample of isolated particles in octadecane with excess oleic acid [non-interacting particles (NIP)] was prepared. The nanocrystal concentration was estimated to be $\sim 10^{12}$ particles/cm³ by sampling a small volume of diluted solution on a TEM grid and roughly counting the nanocrystal density on the TEM grid. Zero-field-cooled magnetization versus temperature of this sample was measured at $H=10$ Oe.

B. Array preparation and characterization

The LB technique was used for nanocrystal array preparation.¹⁷ Two types of arrays were prepared, each with a different average interparticle distance. Both arrays were prepared from a colloidal solution of the iron oxide nanoparticles coated with oleic acid ($\text{C}_{18}\text{H}_{36}\text{O}_2$) and containing some unbound fatty acid between the nanocrystals. The water pH in the LB trough was kept neutral for the first type of arrays. In the second array type the pH of the water in the LB trough was set to 10 by an addition of NaOH solution in order to dissolve more of the fatty acid into the subphase and reduce the separation between the nanoparticles. TEM images [Figs. 1(a) and 1(b)] revealed that the arrays prepared from the colloidal solution on a neutral subphase exhibited an average distance between particle centers of 8.4 ± 1.1 nm, whereas the layers prepared at subphase pH=10 exhibited an average distance between particle centers of 7.6 ± 1.3 nm. For simplicity, the samples will be denoted MICS84 and

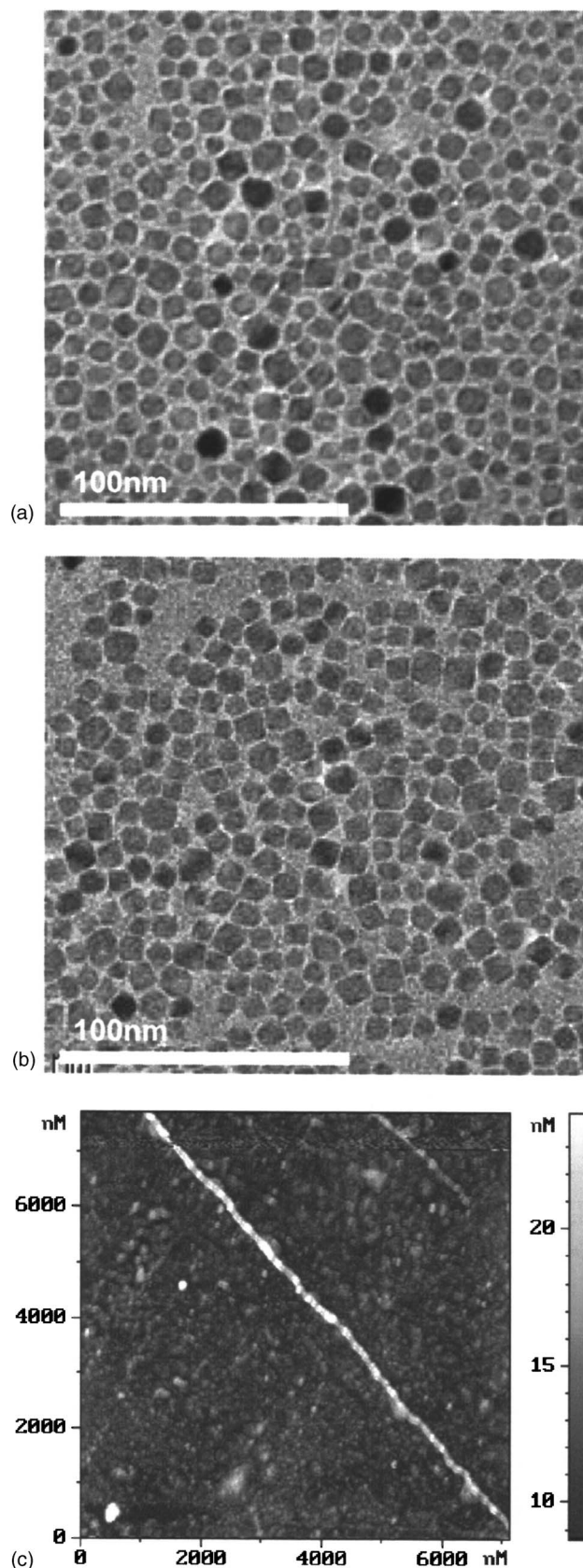


FIG. 1. (a) TEM image of 1 ML MICS84. (b) TEM image of 1 ML MICS76. These images are typical of the samples and extended uniformly over the whole TEM grid. (c) Typical AFM topography image of 1 ML MICS84 deposited on the plastic substrate. The roughness over more than 90% of the area is 5–10 nm.

MICS76 (mean intralayer center-to-center separation 84 and 76 Å, respectively). To obtain arrays of increasing dimension monolayers and multilayers consisting of a number of stacked monolayers of both the MICS84 and the MICS76 samples were prepared. A single monolayer (1 ML), three stacked monolayers (3 ML), five stacked monolayers (5 ML), and ten stacked monolayers (10 ML) of each sample were transferred onto polymer substrates. A 15 ML sample of the MICS74 system was also prepared. The $4 \times 4 \text{ mm}^2$ substrates were cut from a diamagnetic thin polycarbonate sheet.

An atomic force microscope was used to estimate the uniformity of the samples and to ensure satisfactory coverage of the substrates by the arrays. Figure 1(c) is a typical atomic force microscope (AFM) topography image of a 1 ML MICS84 sample deposited on the polycarbonate sheet. Over $> 90\%$ of the area the roughness was 5–10 nm, corresponding to a monolayer, while the rest has higher features consisting of some particles positioned on top of the monolayer as well as excess oleic acid molecules [in the visible line on Fig. 1(c), for example] repelled to the second layer by the high compression of the monolayer ($\sim 30 \text{ mN/m}$). It should be emphasized that over all the 16 mm^2 area of the substrate similar topography was observed. For the multilayer samples larger inhomogeneities were observed. For example, in the 3 ML samples, about 80% of the area had the correct height while the rest was mostly 2 ML and a little 4 ML. Thus, the LB technique was able to achieve far better macroscopic sample uniformity and layer thickness control over techniques such as spin coating and nanocrystal self-assembly, which are typically able to produce uniform arrays on the micrometer scale only.

A solution of concentrated particles with excess fatty acid was dried on a substrate (“drop cast”) as an alternative to the 3D MICS84 sample.

C. Magnetic measurements

All magnetic measurements were performed using a Quantum Design MPMS XL-5 superconducting quantum interference device (SQUID) magnetometer with field applied in the plane of the films. Zero-field-cooled (ZFC) measurements at $H=10 \text{ Oe}$ of the MICS84 and MICS76 samples, of the NIP sample, and of the drop cast sample were carried out to record the blocking temperature as a function of the interparticle distance and the number of layers. A magnetization curve at $T=3 \text{ K}$ was measured on the NIP sample, ac susceptibility as a function of temperature was measured at a frequency range of 0.1–100 Hz and amplitude of 4 Oe on 1, 3, and 10 ML MICS84 samples; 1 and 10 ML MICS76 samples; and on the NIP sample. ac susceptibility with superimposed dc fields of 10, 100, and 1000 Oe as a function of temperature was recorded at 1 Hz on 1, 3, and 10 ML MICS84 samples; 1 and 10 ML MICS76 samples; and on the NIP sample.

III. RESULTS AND DISCUSSION

ZFC magnetization and ac susceptibility versus temperature measurements on the NIP sample revealed that the particles obeyed the Néel-Brown law (Arrhenius-type behavior)

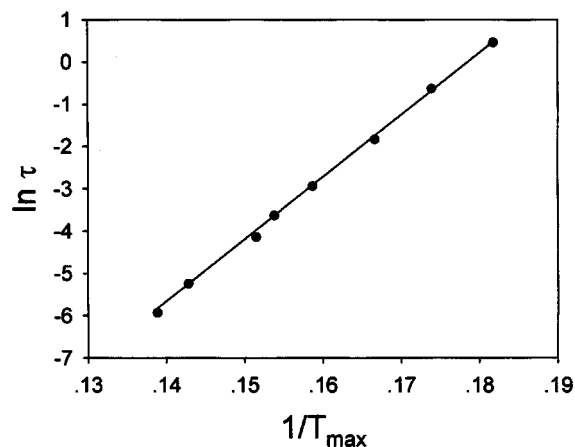


FIG. 2. Fit to the Néel-Brown law of the NIP sample data. $K_a=1.8 \times 10^{-4} \text{ J/m}^3$, $\tau_0=4.1 \times 10^{-12} \text{ s}$.

(Fig. 2). From the fit of the inverse frequency of the ac susceptibility measurement versus its peak temperature to the Néel-Brown expression a low magnetocrystalline anisotropy constant was extracted ($K=1.8 \times 10^4 \text{ J/m}^3$). The bulk anisotropy constants of $\gamma\text{-Fe}_2\text{O}_3$, and magnetite, Fe_3O_4 , are in the range of $(0.5\text{--}1.3) \times 10^4 \text{ J/m}^3$.¹⁸ The blocking temperature (T_b) of the isolated particles deduced from ZFC experiments on nanocrystals at various dilution levels performed with $H=10 \text{ Oe}$ was 20 K. The hysteresis curve for the isolated particles measured at 3 K yielded a coercive field of 100 Oe.

The most straightforward way to estimate the magnitude of dipole-dipole interaction energy in the various samples is to compare their blocking temperatures, which are expected to increase with increasing interaction strength. ZFC measurements of the nanocrystal arrays yielded a set of blocking temperatures corresponding to the different numbers of layers (Table I). The blocking temperatures of the MICS76 samples were higher than those of the MICS84 samples due to the stronger dipolar interactions between the nanoparticles within the layers. The strength of dipolar interactions between the nanoparticles falls as the cube of the distance between the particle centers ($1/r^3$), and is sensitive to the distribution of interparticle distance. The interlayer separation, however, was found to be $\sim 1 \text{ nm}$ by AFM imaging of multilayer samples for both MICS84 and MICS76 arrays. This distance depends on the amount of surfactant dissolved out of the particles' surfaces at the contact area of the nanoparticle surfaces and aqueous subphase before deposition on the substrate and on the thickness of the surfactant layer attached to the nanoparticles opposite to the subphase.

TABLE I. ZFC blocking temperatures of the NIP, MICS84, MICS76, and drop cast samples.

| Sample | $T_b(H=10 \text{ Oe})$ MICS76 | $T_b(H=10 \text{ Oe})$ MICS84 |
|-----------|-------------------------------|-------------------------------|
| NIP | | 20 K |
| 1 ML (2D) | 90 K | 62 K |
| 3 ML | 90 K | 80 K |
| 5 ML | 100 K | 80 K |
| 10 ML | 110 K | 100 K |
| 3D | 110 K (15 ML) | 100 K (drop cast) |

TABLE II. T_{\max} values taken from the $\chi''(T)$ curves measured on several samples at $H=0, 10, 100$ Oe. All measurements were done at 1 Hz, units are K.

| Sample | T_{\max} ($H=0$ Oe) | T_{\max} ($H=10$ Oe) | T_{\max} ($H=100$ Oe) |
|--------------|---------------------------|----------------------------|-----------------------------|
| NIP | 6 | 6 | 6 |
| 1 ML MICS84 | 28 | 30 | 13 |
| 3 ML MICS84 | 63 | 55 | 20 |
| 10 ML MICS84 | 88 | 78 | 27 |
| 1 ML MICS76 | 70 | 64 | 33 |
| 10 ML MICS76 | 93 | 81 | 42 |

The strength of interaction between two neighboring particles within each monolayer array is roughly given by the point dipole-dipole interaction term, μ^2/r^3 , where μ is the average magnetic moment of a particle, and the total dipolar interaction energy (E_{dip}) of a particle should be proportional to this number. A more accurate estimate of E_{dip} in a realistic, disordered array with nonspherical particles should take into account higher multipole interaction terms. The ratio $E_{\text{dip}}(2\text{D MICS84})/E_{\text{dip}}(2\text{D MICS76})$ can thus be estimated as 0.74, not far from the observed ratio: $T_b(2\text{D MICS84})/T_b(2\text{D MICS76})=0.69$. The ratio of $T_b(3\text{D MICS84})/T_b(3\text{D MICS76})$ was 0.9, higher than the E_{dip} ratio for the 2D case. This is probably due to the relatively short interlayer separation, which provides the major contribution to the dipolar energy in the 3D case and thus reduces the differences in the local energy barriers between the two sample types. It is more difficult to evaluate the strength of interparticle interactions in the various array samples with respect to the single-particle anisotropy energy, i.e., the ratio $E_{\text{dip}}/(KV)$, since it is difficult to extract the value of E_{dip} experimentally, or even to calculate it using a point-dipole model. A very rough estimate for this ratio may be obtained from the blocking temperature ratios: $T_b(n\text{ML})/T_b(\text{NIP})$ which is of the order of 3–5 for the various array samples, with n being the number of layers.

The $H=0$ column in Table II displays the temperatures of the peaks (T_{\max}) in the $\chi''(T)$ curves for several samples, measured at ac field frequency of 1 Hz. These follow the general trend observed for the dc ZFC magnetization measurements.

The widths of the $\chi''(T)$ curves also provide information about the strength of interactions in the various samples. In an ensemble of noninteracting magnetic nanoparticles the width of the susceptibility versus temperature curve is typically determined by the distribution of magnetic anisotropy energy barriers of individual particles. Figure 3(a) compares the $\chi''(T)$ curves for the NIP sample and the 1 ML MICS84 and 10 ML MICS84 samples where the temperature axis was scaled by T_{\max} and the susceptibility at the peak normalized to 1. Figure 3(b) compares the scaled curves of the NIP and the 1 ML MICS84 and 1 ML MICS76 samples, while Fig. 3(c) compares the scaled curves of the NIP, and the 10 ML MICS84 and 10 ML MICS76 samples. The significant decrease in the scaled $\chi''(T)$ curve widths (except for the 1 ML MICS84 curve) on going from isolated particles to 1 ML (2D) and 10 ML (effectively 3D) arrays is an indication that

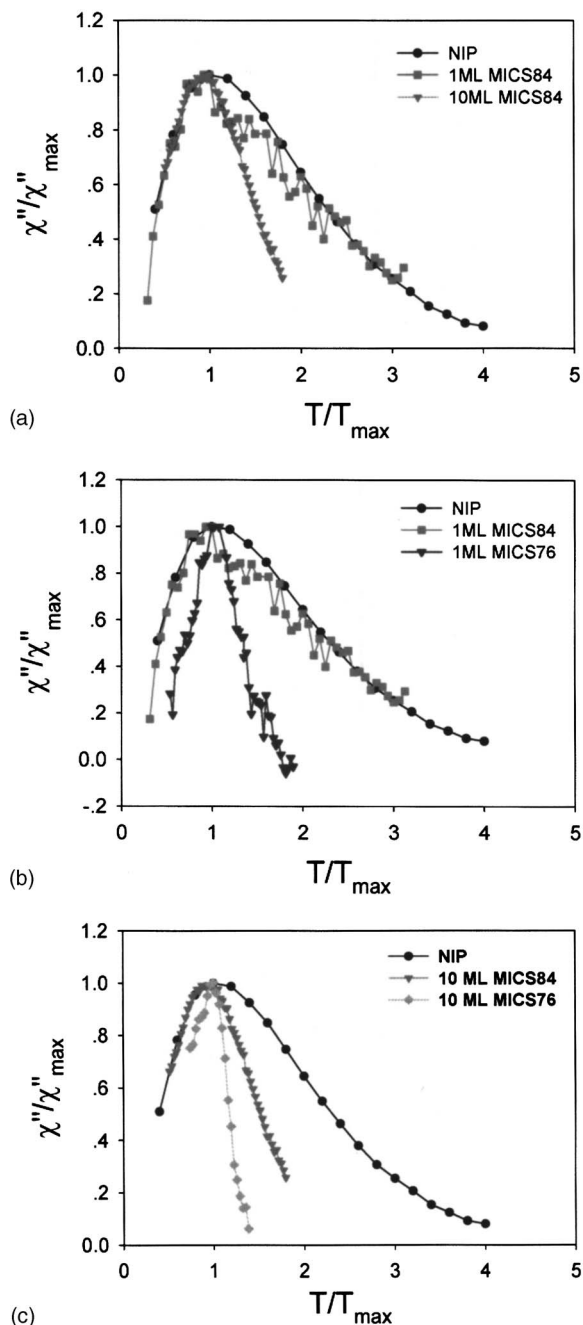


FIG. 3. Scaled χ'' vs scaled T for (a) NIP, 1 ML MICS84, and 10 ML MICS84 samples. (b) NIP, 1 ML MICS84, and 1 ML MICS76 samples. (c) NIP, 10 ML MICS84, and 10 ML MICS76.

in the arrays the individual magnetic particle anisotropies are no longer significant compared with the dipolar interactions. In addition, similar to the blocking temperature data, the differences between the MICS84 and MICS76 curve widths were more pronounced in the 1 ML samples. The 1 ML MICS76 curve width was much smaller than that of the 1 ML MICS84 curve due to the stronger in-plane dipolar interactions in this sample. The 1 ML MICS84 curve had a scaled width closer to the NIP sample, which, together with the smaller shift of T_{\max} , indicates weaker dipolar interactions compared to the other samples.

The χ'' vs T curves were measured for several samples at frequencies between 0.1 and 100 Hz. Figure 4 is an example

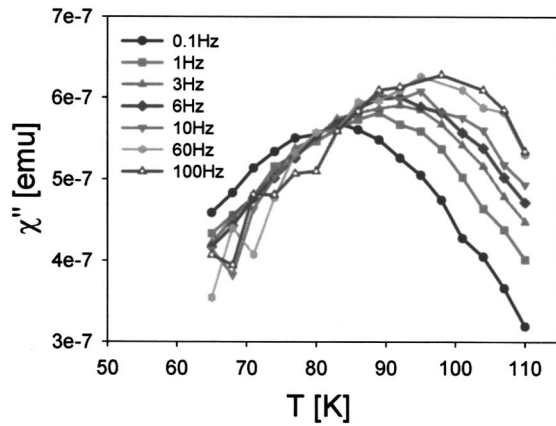


FIG. 4. χ'' vs temperature at different frequencies of the 10 ML MICS84 sample.

of a set of $\chi''(T)$ curves at various frequencies measured for the 10 ML MICS84 system. The relaxation time $\tau = (2\pi f)^{-1}$ as a function of the T_{\max} extracted from the $\chi''(T)$ peaks of each sample was fitted to the scaling law $\tau = \tau^* [T_g / (T_{\max} - T_g)]^{z\nu}$ and to the phenomenological Vogel-Fulcher law $\tau = \tau_0 \exp[E_0/k_B(T_{\max} - T_0)]$. The fit parameters are summarized in Table III. The τ_0 values for the Vogel-Fulcher fits were in the range of 10^{-7} – 10^{-11} s and τ^* values for the scaling law were 10^{-3} – 10^{-6} s for all samples.

The temperature dependence of magnetization dynamics was extensively used as a tool to probe the strength of interactions in magnetic nanoparticle systems. Such data can be used to determine the extent of deviation of the relaxation-time dependence on temperature from the simple Arrhenius type behavior observed for isolated particle magnetization dynamics. For moderately interacting magnetic nanoparticles produced by physical vapor deposition it was found that the Arrhenius law describes well the experimentally observed $\tau(T_{\max})$.⁹ As seen in Fig. 5, the experimental data (circles) in the present work, even that for the 1 ML MICS84, cannot be fitted by the Arrhenius expression (red curve). This implies that the individual particle magnetization cannot be described as switching in an effective potential barrier, rather, the dynamics of the whole ensemble of interacting particles should be considered simultaneously. The empirical Vogel-Fulcher law was often used to describe the slowing down of relaxation found in glasses and spin glasses.¹⁹ As can be seen in Fig. 5, this expression fits well the ac susceptibility data for the 1 ML MICS84 sample (black curve). A fit of comparable quality was also obtained using the scaling law. E_0 , representative of some effective energy barrier experienced

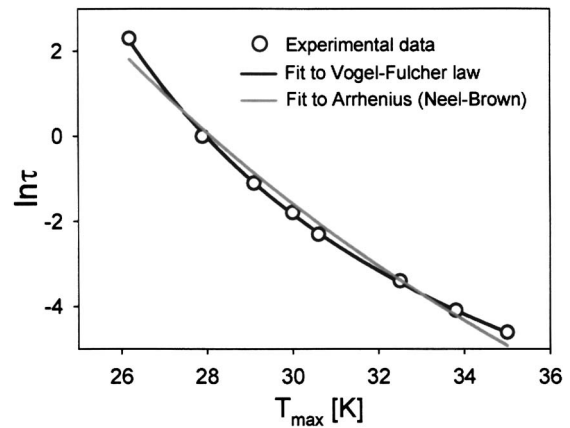


FIG. 5. Fit to the Néel-Brown law (gray curve) and fit to the Vogel-Fulcher law (black curve) of the $\ln \tau$ vs T_{\max} data (circles) obtained from imaginary susceptibility curves of the 1 ML MICS84 sample.

by the magnetization of a characteristic nanoparticle, should scale roughly as the blocking temperature while T_0 (or T_g) is an indicator to a characteristic temperature at which the dynamics becomes collective (glassy).

In conventional spin-glass systems T_g is the temperature of the onset of glass behavior and is characterized by a cusp in the $\chi'(T)$ curve. These systems undergo a thermodynamic phase transition at T_g where a critical slowing down of the relaxation according to the scaling law $\tau = \tau^* [T_g / (T - T_g)]^{z\nu}$ appears. In systems of interacting nanoparticles no cusp appears in the susceptibility and the fitted T_g values merely indicate the temperature range of the onset of slow, glasslike dynamics. The nature of magnetization freezing in these systems is unclear. Memory and aging phenomena were observed in systems of interacting nanoparticles and have been treated using models such as the droplet model²⁰ and hierarchical arrangement of the metastable states.²¹ The scaling law was used to explore the nature of the approach to the glassy state in systems of interacting nanoparticles.^{10,11}

Both T_0 and T_g values increased with the strength of interactions and the number of layers in the sample. For example, the T_g values in the 10 ML arrays in both types of samples were the same ($T_g = 71$ K), and also the T_0 values of these samples were very close (46 K in the MICS76 sample and 42 K in the MICS84 sample) due to the strong interlayer interactions.

The critical exponent $z\nu$ appearing in the scaling law consists of the static exponent ν , and a dynamic part z . The static critical exponent is related to the correlation length of the system: $\xi \propto |t|^{-\nu}$ where $t = T / (T_g - T)$ is the reduced temperature. The $z\nu$ values of the samples provide interesting information about the differences between the MICS84 and MICS76 systems (Table III). The $z\nu$ values in the MICS84 system were ~ 9 – 11 whereas the $z\nu$ values of the MICS76 system were 6.6 and 7. Values of ~ 9 – 11 have been reported for interacting magnetic nanoparticle in frozen ferrofluids¹¹ and arrays,¹³ and a value of 7 was obtained for strongly interacting magnetic nanoparticle powder.⁷ Spin glasses were reported to have a variety of $z\nu$ values: ~ 7 [$\text{CdCr}_2(\text{In})\text{S}_4$],²² 10.2 (AuFe),²³ and 5.5 (CuMn),²³ and the $z\nu$ values obtained for 3D Ising models were ~ 8 (Ref. 22) and 7.2.²³ In the

TABLE III. T_0 values obtained from fits to the Vogel-Fulcher law and T_g and $z\nu$ values of the same samples obtained from fits to the scaling law.

| Sample | T_0 (K) | T_g (K) | $z\nu$ |
|--------------|-----------|-----------|----------|
| 1 ML MICS84 | 16.7±0.1 | 23.0±0.1 | 11.5±0.2 |
| 3 ML MICS84 | 27.3±0.1 | 43.5±0.1 | 8.9±0.1 |
| 10 ML MICS84 | 42.4±0.4 | 71.5±0.3 | 9.0±0.1 |
| 1 ML MICS76 | 34.6±0.1 | 56.3±1.3 | 6.6±0.5 |
| 10 ML MICS76 | 46.5±0.3 | 71.7±0.5 | 7.0±0.2 |

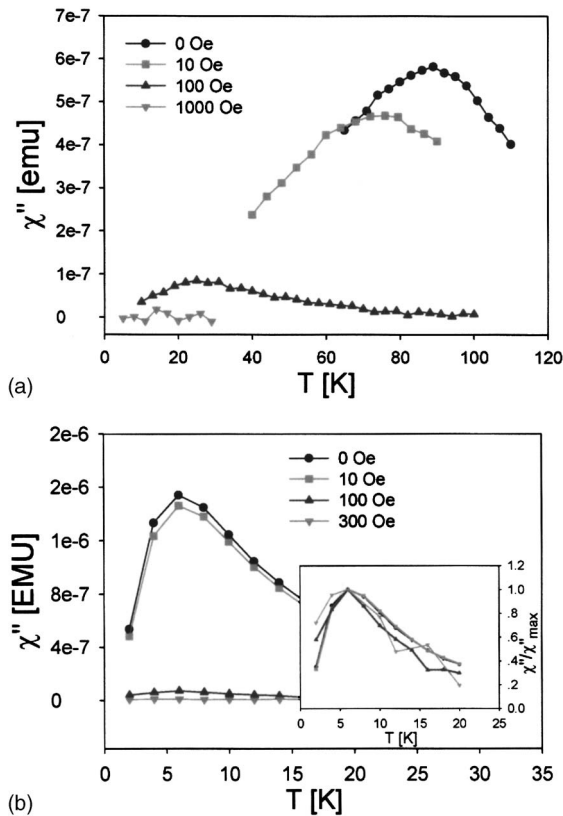


FIG. 6. χ'' vs temperature measured at 1 Hz with superimposed dc fields of the (a) 10 ML MICS84 sample and (b) NIP sample; inset: scaled χ'' vs temperature of the same curves.

present work the value of zV varied between the two types of monolayers with no significant dependence on the dimensionality of the arrays.²⁴ The difference in the critical exponents should therefore arise from the different interaction strengths.

Dormann *et al.* used the ratio $(T_f - T_0)/T_f$ as an indicator to the nature of the transition from a paramagnetic (and superparamagnetic) state to the spin-glass state.¹ T_f (magnetization freezing temperature) was chosen to be T_{\max} at some ac frequency and T_0 was extracted from the Vogel-Fulcher law. For systems undergoing a spin-glass phase transition the value of $(T_f - T_0)/T_f$ was very low (~ 0.07 for CuMn), whereas higher values (~ 0.4) found in systems such as $\text{ZnCr}_{1.6}\text{Ga}_{0.4}\text{O}_4$ (Ref. 1) were characterized by progressive freezing of superparamagnetic clusters. The $(T_f - T_0)/T_f$ values of all the systems studied in the present work (T_f chosen to be T_{\max} at 1 Hz) were ~ 0.4 – 0.6 which is indicative of a gradual magnetization freezing transition rather than a true glass transition. Another alternative to a spin-glass transition is a paramagnetic-to-ferromagnetic-like ordering transition that might occur upon cooling of ordered hexagonal arrays of magnetic dipoles.²⁵ Since the magnetic nanocrystal arrays are characterized by a large difference between T_{\max} and T_0 (or T_g) the probability of local magnetic ordering upon cooling increases.

Measurements of ac susceptibility versus temperature with a superimposed in-plane dc field probe the effect of the external field on the local dipolar interactions. Figures 6(a) and 6(b) show $\chi''(T)$ curves measured at 1 Hz for the 10 ML

MICS84 sample and the NIP sample at different fields. As seen in Table II, with increasing dc field the peak temperature decreased in all nanoparticles' array samples. The curves at $H > 0$ appeared to follow the low-temperature tail of the curve at $H = 0$ Oe. A decrease in the temperatures of the $\chi''(T)$ peak maxima with increasing field was observed for all samples. However, only the curves of the array samples were significantly influenced by a weak field of 10 Oe while the NIP sample hardly responded to this field and the position of T_{\max} for this sample was unaffected by the increase in the dc field. A similar behavior was observed by Jonsson *et al.* in an Fe-C nanoparticles ferrofluid solution²⁶ and in the amorphous metallic spin-glass $(\text{Fe}_{0.15}\text{N}_{0.85})_{75}\text{P}_{16}\text{B}_6\text{Al}_3$.²⁷ At 1000 Oe the susceptibility value became practically zero for all the samples and it was not possible to determine a value for T_{\max} . In all the samples the largest drop in the magnitude of the $\chi''(T)$ peak occurred between $H = 10$ Oe and $H = 100$ Oe. This can be simply explained by the behavior of the magnetization curve where the slope of the magnetization, χ , decreases with increasing field towards saturation. This behavior depends weakly on the interactions between the particles and could therefore be observed both in the interacting and noninteracting systems.

The strong influence of the external dc field, as low as 10 Oe, on the $\chi''(T)$ curves of the nanocrystal arrays is an indication of the formation of domains of strongly interacting particles in the arrays around the blocking temperature and provides further support to the notion of collective magnetization dynamics. At large H (~ 1000 Oe in the present case) all the particle moments became aligned with the dc field, and being fully saturated, they did not respond to the ac field at all. In the NIP system no domains existed and therefore no change was observed in the maxima values of the peaks at different fields.

If one assumes a relatively homogenous dipolar interaction distribution between the particles in the samples then the droplet model could probably describe the effect of the external field. This model has been used to describe the response of spin-glass systems to external fields²⁰ and was adopted to describe the response of interacting magnetic particles to such fields.²⁶ According to this model the correlated spin-glass domain size is reduced with the increase in the dc field, resulting in a decrease in the values of T_{\max} . Alternatively, in case that some of the particles in the arrays are weakly interacting with their neighbors, due to their small size and/or large separation from their nearest neighbors, a different explanation for the external field effect could be invoked. Then, the low-temperature peak observed for the $\chi''(T)$ curves under a dc field would correspond to the small fraction of the weakly interacting particles in the array, while the strongly interacting particles' imaginary susceptibility would be attenuated due to the alignment of their domains close to saturation. In this case, the droplet model might still be applicable to the nanoparticles arrays but, depending on the level of order in the close-packed arrays, an opposite picture could also be possible. In a case of a perfectly uniform hexagonal 2D array magnetically ordered domains may actually increase in size with increasing field, accompanied by a reduction in their magnetic susceptibility.

Luis *et al.* measured the effect of dc fields on sputtered layers of Co particles²⁸ and observed results similar to the present work. They used a model suggested by Jonsson *et al.* to describe the behavior of their system under an external dc field.³ This model exploits the fact that due to size distribution some particles switch more slowly close to T_{\max} . These nanoparticles polarize their smaller superparamagnetic neighbors via an induced local field and as their magnetization switches the smaller moments follow. At low temperatures, however, spin-glass dynamics was dominant and phenomena such as aging were observed. The present results indicate that the stronger interactions existing in the colloidal particle arrays give rise to collective dynamics. Consequently, one is left with two possible models suitable for describing the temperature-dependent dynamics of strongly interacting magnetic nanocrystals—the droplet model describing the magnetization behavior of a spin glass near the glass transition versus ferromagnetic-like ordering of domains of nanocrystals below the blocking temperature. It is difficult to distinguish between the two possibilities with the current samples and measurement techniques. Better-ordered arrays of strongly interacting magnetic nanocrystals may form larger magnetic domains and consequently exhibit distinctly different magnetization behaviors at low temperatures, corresponding to domain-wall motion rather than magnetization switching.

IV. CONCLUSION

The effects of interparticle separation and dimensionality on the dipolar interactions and magnetization dynamics in systems of interacting single-domain iron oxide nanoparticles were studied. The strength of dipolar interactions, indicated by the blocking temperature, increased with the decrease in interparticle separation and the increase in dimension. The interactions between the layers, due to shorter interlayer separation, dominated the magnetization behavior of the multilayer films. Collective, non-Arrhenius, magnetization dynamics was observed in all the samples, even for the 2D MICS84 sample, which exhibited weaker interactions. The temperature dependence of the magnetization relaxation in these arrays indicates gradual freezing of domains of strongly interacting magnetic particle moments, probably without displaying a paramagnetic-to-spin-glass phase transition. The fitted scaling law exponent differed substantially between the MICS76 and MICS84 samples, where increasing interaction strength led to a smaller exponent value. Another manifestation of the strong interactions

in the nanocrystal arrays was the strong shift in the ac imaginary susceptibility peak temperature with application of small dc fields. Both of these results and the value of the $(T_f - T_0)/T_f$ ratio indicate that the interacting magnetic dipoles may be ordered into small, ferromagneticlike domains.

ACKNOWLEDGMENTS

This work was supported by Israel Science Foundation Grant No. 208/03 and the James Frank program.

- ¹J. L. Dormann, L. Bessais, and D. Fiorani, *J. Phys. C* **21**, 2015 (1988).
- ²M. El-Hilo, K. O'Grady, and R. W. Chantrell, *J. Magn. Magn. Mater.* **114**, 307 (1992).
- ³T. Jonsson, P. Nordblad, and P. Svelindh, *Phys. Rev. B* **57**, 497 (1998).
- ⁴M. Jamet, V. Dupuis, P. Melinon, G. Guiraud, A. Perez, W. Wernsdorfer, A. Traverse, and B. Baguenard, *Phys. Rev. B* **62**, 493 (2000).
- ⁵G. A. Held, G. Grinstein, H. Doyle, S. Sun, and C. B. Murray, *Phys. Rev. B* **64**, 012408 (2001).
- ⁶C. Petit, S. Rusponi, and H. Brune, *J. Appl. Phys.* **95**, 4251 (2004).
- ⁷D. Fiorani, J. L. Dormann, R. Cherkaoui, E. Tronc, F. Lucari, F. D'Orazio, L. Spinu, M. Noguez, A. Garcia, and A. M. Testa, *J. Magn. Magn. Mater.* **197**, 143 (1999).
- ⁸D. Farrell, Y. Cheng, Y. Ding, S. Yamamuro, C. Sanchez-Hanke, C. C. Kao, and S. A. Majetich, *J. Magn. Magn. Mater.* **282**, 1 (2004).
- ⁹F. Luis, F. Petroff, J. M. Torres, L. M. Garcia, J. Bartolome, J. Carrey, and A. Vaures, *Phys. Rev. Lett.* **88**, 217205 (2002).
- ¹⁰P. Jonsson, M. F. Hansen, P. Svelindh, and P. Nordblad, *J. Magn. Magn. Mater.* **226–230**, 1315 (2001).
- ¹¹C. Djurberg, P. Svelindh, and P. Nordblad, *Phys. Rev. Lett.* **79**, 5154 (1997).
- ¹²M. F. Hansen, P. E. Jonsson, P. Nordblad, and P. Svelindh, *J. Phys.: Condens. Matter* **14**, 4901 (2002).
- ¹³P. Poddar, T. Telem-Shafir, T. Fried, and G. Markovich, *Phys. Rev. B* **66**, 060403 (2003).
- ¹⁴S. Sun, H. Zeng, D. B. Robinson, S. Raoux, P. M. Rice, S. X. Wang, and G. Li, *J. Am. Chem. Soc.* **126**, 273 (2004).
- ¹⁵J. Park, K. An, Y. Hwang, J. G. Park, H. J. Noh, J. Y. Kim, J. H. Park, N. M. Hwang, and T. Hyeon, *Nat. Mater.* **3**, 891 (2004).
- ¹⁶J. Tang, M. Myers, K. A. Bosnik, and L. E. Brus, *J. Phys. Chem. B* **107**, 7501 (2003).
- ¹⁷T. Fried, G. Shemer, and G. Markovich, *Adv. Mater. (Weinheim, Ger.)* **13**, 1158 (2001).
- ¹⁸A. T. Ngo and M. P. Pileni, *New J. Phys.* **4**, 87 (2002).
- ¹⁹S. Shtrikman and E. P. Wohlfarth, *Phys. Lett.* **85A**, 467 (1981).
- ²⁰D. S. Fisher and D. A. Huse, *Phys. Rev. B* **38**, 373 (1988).
- ²¹F. Lefloch, J. Hamman, M. Ocio, and E. Vincent, *Europhys. Lett.* **18**, 647 (1992).
- ²²I. A. Campbell, *Phys. Rev. B* **37**, 9800 (1988).
- ²³J. Souletie and J. L. Tholence, *Phys. Rev. B* **32**, 516 (1985).
- ²⁴P. Nordblad, *J. Phys.: Condens. Matter* **16**, S715 (2004).
- ²⁵V. Russier, *J. Appl. Phys.* **89**, 1287 (2001).
- ²⁶P. E. Jonsson, S. Felton, P. Svelindh, P. Nordblad, and M. F. Hansen, *Phys. Rev. B* **64**, 212402 (2001).
- ²⁷P. Svelindh, L. Lundren, P. Nordblad, and H. S. Chen, *Europhys. Lett.* **3**, 243 (1987).
- ²⁸F. Luis, F. Petroff, and J. Bartolome, *J. Phys.: Condens. Matter* **16**, 5109 (2004).